Surfactant Protein A (SP-A) inhibits agglomeration and macrophage uptake of toxic amine modified nanoparticles

Zofi McKenzie[1*], Michaela Kendall[1,2*], Rose-Marie Mackay[1], Harry Whitwell[1], Christine Elgy[2], Ping Ding[3], Sumeet Mahajan[4,5], Cliff Morgan[6], Mark Griffiths[6], Howard Clark[1,4,7] and Jens Madsen[1,4,7]

1 Child Health, Human Development and Health, Faculty of Medicine, University of Southampton, Southampton General Hospital, Southampton SO16 6YD, United Kingdom.

2 School of Geography, Earth and Environmental Sciences University of Birmingham, Birmingham, B15 2TT, United Kingdom.

3 Facility for Environmental Nanoscience Analysis and Characterisation (FENAC), School of Metallurgy and Materials, University of Birmingham, Birmingham, B15 2TT, United Kingdom.

4 Institute for Life Sciences, University of Southampton, Highfield, Southampton, SO17 1BJ, United Kingdom.

5 Department of Chemistry, University of Southampton, Highfield, Southampton, SO17 1BJ, United Kingdom.

6 Leukocyte Biology, Royal Brompton Campus, Imperial College London, London, SW3 6NP, United Kingdom.

7 National Institute for Health Research, Southampton Respiratory Biomedical Research Unit, Southampton Centre for Biomedical Research, University Hospital Southampton NHS Foundation Trust, Southampton, SO16 6YD, United Kingdom.

*Both authors contributed equally to the manuscript.

Keywords: Nanoparticles, surfactant, mucosal, collectin, surface chemistry

Address for correspondence:

Jens Madsen PhD

Child Health,

Sir Henry Wellcome Laboratories

Human Development and Health,

Faculty of Medicine,

University of Southampton,

Southampton General Hospital,

Tremona Road,

Southampton
SO16 6YD.
United Kingdom.
Phone: +44238124940
Email: j.madsen@southampton.ac.uk

Abstract

The lung provides the main route for nanomaterial exposure. Surfactant protein A (SP-A) is an important respiratory innate immune molecule with the ability to bind or opsonise pathogens to enhance phagocytic removal from the airways. We hypothesised that SP-A, like SP-D, may interact with inhaled nanoparticulates and that this interaction will be affected by nanoparticle surface characteristics. Here we characterize the interaction of SP-A with unmodified (U-PS) and amine-modified (A-PS) polystyrene particles of varying size and zeta potential using Dynamic Light Scatter analysis. SP-A associated with both 100 nm U-PS and A-PS in a calcium independent manner. SP-A induced significant calcium dependent agglomeration of 100 nm U-PS nanoparticles but resulted in calcium independent inhibition of A-PS self agglomeration. SP-A enhanced uptake of 100 nm U-PS into macrophage-like RAW264.7 cells in a dose dependent manner but in contrast inhibited A-PS uptake. Reduced association of A-PS particles in RAW264.7 cells following pre-incubation of SP-A was also observed with coherent anti-Stokes Raman spectroscopy (CARS). Consistent with these findings, alveolar macrophages from SP-$A^{-/-}$ mice were more efficient at uptake of 100 nm A-PS compared to wildtype C57Bl/6 macrophages. No difference in uptake was observed with 500 nm U-PS or A-PS particles. Pre-incubation with SP-A resulted in a significant decrease in uptake of 100 nm A-PS in macrophages isolated from both groups of mice. In contrast, increased uptake by alveolar macrophages of U-PS was observed after pre-incubation with SP-A. Thus we have demonstrated that SP-A promotes uptake of non-toxic U-PS particles but inhibits the clearance of potentially toxic A-PS particles by blocking uptake into macrophages.

Introduction

The ability of nanotechnology to produce engineered nanoparticles (NPs) of various shapes and materials has opened up new applications in areas such as medicine, engineering, electronics, textiles and cosmetics. The number of consumer products containing nanoparticles is rapidly increasing and is now counted in thousands (Nanotechnologies, 2014). This reflects the unique and diverse properties of nanomaterials, which can be very different from the bulk material due in part to their enhanced surface to mass ratio (Oberdorster et al., 2005).

Exposure to nanomaterials is not a new phenomenon. Throughout evolution humans have been exposed to nanosized particles from both biogenic and anthropogenic sources. However, human lung exposures have risen dramatically due to anthropogenic emission from diesel engines, power stations and engineering processes optimised for manufacturing nanoscale materials (Oberdörster et al., 2005). Due to the small size of nanomaterials, they are often airborne and have the capability of reaching the alveolar compartment of the lungs (Oberdörster et al., 2005, Oberdorster et al., 2002). Once inside the airways, the NPs can be adsorbed onto the mucosal surface in the upper airways and into surfactant lining the lower airways. A nano-bio corona of biological molecules then forms on the NP surface which can in turn influence the clearance, bioavailability and potential toxicity of the NPs (recently reviewed in (Kendall and Holgate, 2012)).

Pulmonary surfactant is a multi-layered lipoprotein substance, comprising approximately 90% lipids and 10% protein, and lines the alveolar epithelium at the air liquid interface. Pulmonary surfactant performs two vital functions in the lung; reducing alveolar surface tension and protecting the lung from microbial infection (reviewed in (Pérez-Gil, 2008)). Surfactant protein A (SP-A) and its sister protein SP-D are both hydrophilic proteins found in surfactant belonging to the calcium dependent (C-type) lectin sub-family known as ‘collectins’ (*coll*agenous *lectins*). Collectins are oligomeric proteins made up of trimeric units. The trimeric units are composed of three monomers, each with its own carbohydrate recognition domain (CRD) containing the lectin activity (**Fig S1**). The trimeric units are characterised by four structural domains; an amino terminus (where the oligomerization between trimeric units take place), a collagenous domain, a neck region and the CRD region. Six of these trimeric units oligomerize to form octadecamers, the native form of SP-A

(Fig S1). As SP-A has a bend in the collagenous region the quaternary structure has been described as a “bunch of tulips” similar to the complement C1q molecule (Voss et al., 1988). Four trimeric units come together to form SP-D in the shape of a cross (**Fig S1**). SP-A is the most abundant of the two proteins with approximately ten times more SP-A in surfactant than SP-D (Pastva et al., 2007). The pulmonary collectins, SP-A and SP-D, play an important role in the innate immune defence of the lung; they are pattern recognition molecules and are able to protect the lung from infection through a variety of mechanisms. They recognise and bind specific carbohydrate moieties on the surface of micro-organisms via the CRD and can facilitate microbial clearance through agglutination and opsonisation (reviewed in (Pastva et al., 2007)). They also promote uptake and clearance of dead and dying apoptotic cells in the airway and bind to cell-surface exposed and free DNA debris (Clark et al., 2002, Palaniyar et al., 2003). Both SP-A and SP-D rapidly promote microbial uptake into phagocytes and have anti-inflammatory effects by inhibiting cytokine and chemokine responses of phagocytes and lymphocytes after initial infection. Phagocytosis is believed to keep the phagocytosed material contained and the lung in an inflammation-free and quiescent state for optimal lung function (Borron et al., 1996, Borron et al., 1998, Borron et al., 2000, Hansen et al., 2007, Brinker et al., 2003). *In vivo* studies with mice deficient for SP-A (SP-A-/- mice) have shown that SP-A is important for the phagocytosis and clearance of both bacteria and viruses from the lung (LeVine et al., 1997, LeVine et al., 1998, LeVine et al., 1999b, LeVine et al., 1999a, LeVine et al., 2002, Li et al., 2002). Recent studies have suggested that SP-A and SP-D also play a role in the clearance of non-infectious particulate matter in the lung (Kendall et al., 2013, Ruge et al., 2011, Ruge et al., 2012).

We have previously characterised the interaction of SP-D with various nanoparticles including unmodified (U-PS) and amine (A-PS) surface modified polystyrene particles (Kendall et al., 2013). SP-D co-localized to 200 nm A-PS (A-PS) NPs in A549 epithelium cells *in vitro* (Kendall et al., 2013). Furthermore, alveolar macrophages from wild type (WT) C57Bl/6 mice showed enhanced uptake of both 100 nm and 500 nm U-PS and A-PS particles compared to alveolar macrophages isolated from mice deficient in SP-D (SP-D-/- mice) (Kendall et al., 2013). Addition of exogenous SP-D to alveolar macrophages from SP-D-/- mice enhanced the

percentage of alveolar macrophages taking up 100 nm A-PS (Kendall et al., 2013). Both SP-A and SP-D have been found to bind to carbon nanotubes (Salvador-Morales et al., 2007). The binding was calcium dependent and was variable between batches of nanotubes indicating that the binding was mediated by surface impurities or chemical modifications of the nanotubes (Salvador-Morales et al., 2007). Differential interaction of SP-A was also observed with metal oxide nanoparticles, including titanium oxide and cerium oxide particles, where differences were seen with different surface modified particles derived from the same bulk-material highlighting the importance of the particle size, surface charge and chemistry (Schulze et al., 2011). SP-A has also been found to bind to certain surface modified magnetic nanoparticles (Ruge et al., 2011). It was shown that SP-A specifically interacted with magnetic nanoparticles modified with starch, carboxymethyldextran, chitosan, poly-maleic-oleic acid and phosphatidylcholine compared to bovine serum albumin (Ruge et al., 2011). Surfactant protein A also enhanced the association of the surface modified magnetic particles to alveolar macrophages, except for starch, when compared to BSA. Furthermore, SP-A increased the uptake of phosphatidylcholine nanoparticles into alveolar macrophages whereas the presence of BSA resulted in a decrease in particles taken up by the cells (Ruge et al., 2011). SP-A was also found to facilitate the uptake of aggregated nanoparticle sized tacrolimus complexes, (an immunosupressive agent) into human macrophage-like U937 cells

Here we characterise the interaction of SP-A with polystyrene nanoparticles with well-defined different surface characteristics and size. As in previous studies with SP-D, we focused on U-PS and A-PS at 100, 200 and 500 nm. We characterized the effect of SP-A on uptake of nanoparticles in the murine macrophage cell line RAW264.7 before extending the results into primary alveolar macrophages isolated from SP-A deficient mice and C57Bl/6 wildtype control mice. The effects of interaction of SP-A and NPs are distinct from our previous report for SP-D.

Materials and methods

Nanoparticles (NPs)

Polystyrene particles with and without surface modification with sizes of 100 nm, 200 nm and 500 nm were purchased (Polysciences Inc or Sigma-Aldrich, UK). The particles were unmodified polystyrene (U-PS), amine modified polystyrene (A-PS) and carboxylate modified polystyrene (C-PS). Fluorescent green 100 nm U-PS and fluorescent orange 100 nm A-PS were purchased from Polysciences and Sigma-Aldrich respectively.

SP-A purification

Human bronchoalveolar lavage (BAL) was obtained from patients with written informed consent undergoing lung washings for therapeutic purposes including pulmonary alveolar proteinosis. The procedure was approved by the London National Health Service Research Ethics Committee (NRES reference 10/H0504/9). Native human SP-A was purified from the SP-A rich BAL pellet either by gel chromatography or butanol extraction as described previously (Suwabe et al., 1996, Wright et al., 1987). The purity of SP-A was verified by SDS-PAGE, Western blotting and N-terminal sequencing. The purified SP-A protein was diluted with nanopure water or TBS with 2-5 mM calcium before mixing with particles.

Characterization of the NP and SP-A interaction by Dynamic Light Scatter (DLS) analysis and Zeta Potential (ZP)

The interaction between SP-A and NPs was characterised by DLS (HPPS and Zetasizer Nano ZS, Malvern Instruments, UK) and ZP (Zetasizer Nano ZS, Malvern Instruments). This was initially performed in nano pure water as described previously (Kendall et al., 2013). The DLS and ZP analyses were also performed in Tris buffered saline (TBS) and serum free RPMI-1640 medium without phenol red (Gibco, Life Technologies, UK). In these experiments, A-PS or U-PS particles were suspended in TBS with 5 mM calcium at a concentration of 12.5 cm^2/mL. These particles were diluted with equal volumes of protein (SP-A or BSA) suspended in TBS + calcium at 50 µg/mL. The size and zeta potentials of these suspensions were measured immediately before (T-2) and after (T0) the addition of protein. The particle suspensions were then incubated at 37°C for 48 minutes, the size and ZP were then measured before (T48) and after (T60) the addition of serum free (SF) RPMI. This

yielded a TBS/RPMI ratio of 2:3 and final concentrations of proteins and particles of 10 μg/mL and 2.5 cm^2/mL respectively. The size and ZP of the suspensions were measured again following incubation for a further 2 hours at 37°C (T180). All measurements were conducted at 37°Cusing reusable or disposable capillary cells (Malvern Instruments).

RAW cells

RAW264.7 cells are a mouse macrophage-like cell line established from murine tumours induced with Abelson leukaemia virus (Raschke et al., 1978). Cells were routinely grown in RPMI 1640 (Gibco) supplemented with 1% L-glutamine (Gibco), 1 % Penicillin/Streptomycin (Gibco) and 10% heat inactivated foetal calf serum (Sigma-Aldrich) at 37^oC in a humidified atmosphere with 5% CO_2. The semi-adherent cell line was routinely sub-cultured using a cell scraper every third day.

Uptake of unlabelled A-PS NPs.

RAW264.7 cells were scrapped and plated in 6 well plates on sterile cover slips with 500,000 cells/well. The cells were allowed to adhere for 24 hours and then the cells were incubated with 5 μL of NPs (in general 10^{13} NPs/mL corresponding to $5x10^{10}$ NP/well) in a total volume of 1 mL serum free (SF) RPMI medium for 2 hours. The cells were washed carefully with PBS twice and then fixed in 1% paraformaldehyde in PBS for 1 hour at room temperature. The cover slips, with attached cells, were mounted on a glass side upside down and the edges sealed with clear nail polish. The slides were then analysed using Coherent anti-Stokes Raman scattering (CARS)..

Uptake of fluorescent A-PS and U-PS particles in RAW cells

Aliquots of 100 nm fluorescent orange A-PS or fluorescent green U-PS particles were mixed with SP-A in TBS containing 5 mM calcium to yield concentrations of 9.4 cm^2/mL particles and 25 μg/mL proteins. Particle-protein suspensions were incubated for 1 hour at 37°C in 96 well round bottom plates. RAW264.7 cells were washed three times in SF RPMI and dissociated from culture flasks using a cell scraper. Cells were suspended in SF RPMI at a concentration of $1.67x10^6$ cells/mL and 30 μL aliquots were added to each well yielding a final particle concentration of 3.75cm^2/mL and a TBS/RPMI ratio of 2:3. The cells were incubated for 1 hour at 37°C in a humidified atmosphere. The cells were washed once in 1mL PBS and centrifuged at 400g for 10 minutes to remove excess particles. The cells were resuspended in 40 μL PBS and kept on ice prior to analysis. Trypan blue was added to

the cells immediately before the analysis of 5000 cells per sample using flow cytometry (BD FACS Aria).

Coherent anti-Stokes Raman scattering (CARS) Analysis

CARS microscopy is a label-free chemical imaging technique, which generates contrast using molecular vibrations which are specific to an individual molecule (Patel et al., 2013). A home-built CARS setup comprising of a Chameleon (Coherent) and Compact OPO (APE Berlin) coupled to an inverted Nikon Ti-U 2000 microscope was used to acquire images. The beams were temporally overlapped using a delay stage and combined to form a spatially overlapped collinear beam. The pump beam was set to 835 nm and the Stokes beam from the OPO was tuned to target the Raman frequency of 2850 cm^{-1} to target the CH_2 stretching band. Due to the higher concentration of CH_2 bonds in polystyrene beads and the fact that CARS has a quadratic dependence on the number of oscillators, the PS particles offer high contrast to enable qualitative and quantitative analysis. Amine-modification of the surface of a polystyrene bead will not affect the bulk of the -CH_2 CARS signal (at 2850 cm^{-1}) from the 200 and 500 nm beads used in this work and changes, if any, are well within the spectral resolution of the system.

A series of images was taken for every time point and each individual cell sample. Dwell times of 30 μs were usually chosen and an area of 30 μm x 30 μm scanned at 1024 x 1024 pixels to generate a highly resolved image. Images were acquired with a 40x (NA: 1.2) water immersion objective (Nikon). 4 images were acquired at random on cell areas on the glass coverslip for each separate treatment. In separate experiments to characterize the spatial (lateral) resolution of the CARS microscope beads of various sizes (100-1000 nm) were imaged. It was found that 200 nm sized PS particles were resolvable and hence, the quantitative analysis based on CARS was carried out ≥200 nm beads. At the above target vibrational frequency of 2850 cm^{-1} the PS particles showed up as highly CARS active areas which were quantified using a code written in MATLAB (Mathworks, UK). The number of pixels with intensities exceeding a certain threshold (defined by the background) was counted. This area contributing to the signal is related directly to the number of nanoparticles due to the nature of the CARS signal generation process (multiphoton and hence, inherently confined to the focal plane) and the images presented in this work are 2D rather than

3D projections/stacks. This number corresponding to the bright areas was compared to the overall cell area in pixels to obtain a ratio of NP over cell area.

Mouse Bronchoalveolar Lavage (BAL) and isolation of Alveolar Macrophages

Wild type (WT) C57Bl/6 mice and SP-A deficient mice (SP-$A^{-/-}$, (Li et al., 2002)), back-crossed at least ten times onto the C57Bl/6 mouse background, were housed in specific pathogen free housing at the Biomedical Research Facility at the University of Southampton. Mice received sterile rodent chow and water ad libitum with a 12 hour light and dark cycle. All animal procedures were approved by university local animal ethics committee and the Home Office, United Kingdom. The mice were sacrificed by CO_2 asphyxiation prior to cannulation of the trachea with a fine bore cannula. The BAL was performed by instillation and withdrawal of 3 x 1 mL of PBS with 0.5 mM EDTA, which was subsequently pooled. Cells were pelleted by centrifugation at 300g for 10 min. The cell pellet was re-suspended in SF RPMI. Differential cell counts on cytospin preparations after staining with Diff-Quick (Scientific Products, McGaw Park, IL) confirmed that more than 95% of the cells isolated this way were alveolar macrophages (AMs).

Alveolar macrophage uptake* of *Fluorescent Microspheres

The NPs used in the *ex-vivo* experiments were either 100 nm or 500 nm U-PS (Sigma-Aldrich) or A-PS (Sigma-Aldrich) and were labelled with green fluorescent dye (Fluorescein isothiocyanate (FITC), Sigma-Aldrich) dissolved in carbonate buffer (Sigma-Aldrich) at pH 9.6 at a conc of 1 mg/mL. The FITC was then diluted 1:10 in nanopure water containing the nanoparticles and incubated at room temperature for 1 hour with rotation. The NPs were centrifuged for 10 min at 20,937g and washed twice with nanopure water. We have previously shown that the coupling of FITC to the NPs by this methodology only provides minimal leaching at pH 7.4 and 4.0, to mimic the conditions of the extracellular and endosomal environments, respectively (Kendall et al., 2013). Alveolar macrophages were isolated from C57Bl/6 and SP-$A^{-/-}$ mice as described above, the cells were washed and then incubated with NPs (1:5; 25,000 cells:125,000 NPs), after 5 min sonication, at 37°C for 30 min. The cells were centrifuged at 300g for 10 min and washed 3 times with RPMI Gibco) to remove excess beads and re-suspended in cytofix (BD bioscience) containing 0.2% trypan blue, to quench extracellular fluorescence as previously described (Hartshorn et al.,

1994). The fixed cells were then analysed by fluorescence-activated cell sorting (FACS).

The effects of SP-A on Alveolar macrophage uptake* of *Fluorescent Microspheres

Fluorescent A-PS (Sigma-Aldrich) or U-PS 100 nm nanoparticles (Polysciences) were used to determine the effects of exogenous SP-A on nanoparticle uptake in AMs isolated from C57Bl/6 wild type and SP-$A^{-/-}$ mice as described above. NPs were prepared as described in the section for the "**Uptake of fluorescent A-PS and U-PS particles in RAW cells" and incubated for** 90 minutes at 37°C, 5% CO_2. 17,000 AMs in colorless RPMI were added to the SP-A/NP preparation and incubated for a further 90 minutes at 37°C, 5% CO_2. Cells were then washed with PBS with 1% BSA and 5 mM EDTA (FACS buffer) and centrifuged at 400 g for 10 minutes to remove excess particles. The cells were then re-suspended in FACS buffer containing 0.2% trypan blue for FACS analysis.

FACS Analysis

The FACS analysis was performed on a FACS Aria machine (BD Sciences). Both forward and side scatter threshold values were set to 200 to exclude free beads and cell debris from the analyses. Between 5,000 - 10,000 cells were counted for each sample. The cells that contained beads (FL-1 > ~50) were counted through gating and analysed using BD FACSDiva software v4.3.

Statistical Analysis

Collected data were normal distributed and the parametric unpaired t-test with the Holm-Sidak method was used for testing between two groups and ANOVA (with Bonferoni post hoc test) was used to test results between multiple groups. Data was analysed using SPSS version 20 or Graphpad Prism version 6. Results were considered statistical significant when $p < 0.05$.

Results

We have previously measured the size distributions and zeta potential of a range of similarly sized polystyrene particles (A-PS, C-PS, U-PS) , silicone particles (200V and R816) and carbon black particles (CB400R) in water over time with the addition of purified human SP-D (Kendall et al., 2013). These results showed that SP-D interacted differently with these particles. Here we present the interaction of A-PS and U-PS particles with purified human SP-A.

The size distribution of purified human SP-A in water was measured by light intensity and number. The SP-A preparation was polydispersed with 2 peaks between 10 and 500 nm. A few macromolecules were also evident in this preparation with a small peak around 4500 nm. The majority of the human SP-A, measured by number of particles, showed a median of 30 nm in size (**Fig S2**). The zeta potential of SP-A alone in water was -11.8 mV.

In order to fully characterise the effect of SP-A on particle size and zeta potential these measurements were taken in nanopure water and the media used for cell experiments (i.e. TBS/RPMI).

Firstly, we examined the hydrodynamic size and zeta potentials of A-PS and U-PS particles in nanopure water without calcium with and without the addition of SP-A (**Table S1**). In nanopure water, A-PS particles had a strong positive (+60 mV) zeta potential which became negative with the addition of SP-A (-22.8 mV). U-PS particles had a zeta potential of -38.5 mV which moved closer to zero following the addition of SP-A (-18.7 mV). The z average increased for both A-PS (49.1%) and U-PS (14.3%) particles when incubated with SP-A for 1440 mins (**Table S1**).

The extent of the increase in the z average for 100 nm U-PS particles when incubated with SP-A for 24 hours is indicative of the formation of a protein corona rather than particle agglomeration. Calcium is essential for the lectin activity of SP-A as the ion is involved in the coordination of several of the amino acid residues involved in binding to carbohydrates (Head et al., 2003). We therefore investigated the effect of calcium concentration on the agglomeration rate of 100 nm U-PS particles within a range of from 0 – 2 mM to elucidate if the CRD in SP-A could be involved in agglomeration. The results showed that the agglomeration rate of U-PS depended on the calcium concentration with the addition of 2 mM of calcium required for SP-A mediated agglomeration to occur (**Fig S3B**). When the calcium concentration was 1 mM or lower, agglomeration of U-PS particles in the presence of SP-A was not

observed.. In the presence of 2 mM calcium, SP-A agglomerated the U-PS particles within 10 min and the agglomerates increased in size over time (**Fig S3C**). Based on these results, a minimum concentration of 2 mM $CaCl_2$ was used in the following experiments.

In order to maintain the calcium concentration above 2 mM at all stages of the *in vitro* cellular experiments the particles were pre-incubated with SP-A in tris buffered saline containing 5 mM calcium before the addition of cells suspended in SF RPMI media. The proportion of TBS to RPMI used in the experiments (2:3) was pre-determined not to cause precipitation of calcium – which occurred following the addition of 2 mM calcium directly to RPMI. The size and zeta potentials were measured in TBS or TBS/RPMI at various time points (T-2 to T180). These results are presented in Table 1, Figure 1 and Figure 2. The time points chosen reflect the incubation periods for the *in vitro* cellular experiments. Size and ZP were measured in TBS + Ca immediately before (T-2) and after (T0) the addition of protein. The particle-protein suspensions were incubated at 37°C and the size distributions and ZP measured before (T48) and after (T60) the addition of RPMI. This incubation period reflected the pre-incubation of particles and proteins before the addition of cells. The particle suspensions were incubated again for a further 2 hours to reflect the incubation period with the cells (T180).

Interestingly, the incubation of A-PS particles in TBS/RPMI (T60) resulted in the self agglomeration of the particles at physiological temperatures (i.e. 37°C); pre-incubation with SP-A resulted in a reduction in the A-PS particle self agglomeration at this temperature. BSA also inhibited this self agglomeration (**Fig 1A and Table 1**). The particle size distributions show that SP-A reversed the self agglomeration of A-PS particles over time (**Fig 1B**). However, this did not seem to be the case when examining the Z-average of the particles (**Table 1**). This may be related to the high polydispersity of the samples and the presence of a few large agglomerates skewing the z average. The incubation of SP-A with U-PS particles for 60 minutes at 37°C greatly enhanced the particle size (**Fig 1C**). The incubation of BSA with U-PS particles resulted in a slight increase in the size of the majority of particles and the generation of a small number of larger particle agglomerates around 500 nm in size. At T180 U-PS particles had begun to self agglomerate, a process which was inhibited in the presence of BSA. This was evident by examining both the z average and the

size distribution by number. RPMI promoted the agglomeration of both particles (see **Table 1**).

A-PS particles had a positive zeta potential in TBS with calcium, which reduced slightly over time at 37°C. The addition of RPMI to the A-PS particles resulted in a negative zeta potential (**Table 1**). The addition of SP-A or BSA to the A-PS particles also resulted in negative zeta potentials **(Table 1).** The U-PS particle zeta potential became closer to zero over time and following the addition of RPMI (**Table 1**). The addition of SP-A or BSA had similar effects in making the U-PS zeta potentials closer to zero **(Table 1)**.

Due to the large polydispersity indices for the DLS measurements and the differing results when comparing particle agglomeration kinetics, fluorescence microscopy was also used to examine nanoparticle agglomeration in buffered saline with or without calcium following incubation with SP-A or BSA. The micrographs show that the U-PS particles remained stable either in the presence or absence of calcium at physiological temperatures (**Fig 2**). The incubation of U-PS particles with SP-A in the absence of calcium resulted in a small degree of particle agglomeration, however, this agglomeration was greatly enhanced in the presence of 2 mM calcium and SP-A (**Fig 2**). In order to ascertain whether the effect was specific to SP-A, we performed the experiment with a similar concentration of BSA and observed no agglomeration with or without the presence of calcium (**Fig 2**). A-PS particles self-agglomerated at physiological temperatures (i.e. 37°C). This self-agglomeration was inhibited in the presence SP-A in a calcium independent manner. However, large agglomerates were still evident when A-PS particles were incubated with BSA (**Fig 2**).

The association of SP-A with A-PS and U-PS particles was also examined using sodium dodecyl sulfate polyacrylamide gel electrophoresis (SDS-PAGE) analysis. Particles were incubated with SP-A for 24 hours at 37°C in TBS containing calcium or EDTA. The particles were then centrifuged and washed twice in the appropriate buffer (i.e. TBS containing Ca or EDTA) and the pellet examined using reduced SDS-PAGE. This allowed the determination of the hard (i.e. strongly bound) SP-A corona. SP-A strongly associated to U-PS particles and the association independent of calcium. SP-A was found not to strongly associate with the A-PS particles wither in the presence of calcium or EDTA (see **Fig S4**).

Toxicity of U-PS and A-PS NPs

In order to establish whether particle toxicity could influence cellular uptake of the particles the effect of the NPs on cellular toxicity was investigated using the tetrazolium dye (MTT) colorimetric assay for cellular growth and viability. RAW264.7 cells were incubated with A-PS and U-PS particles in a range from 1-15 cm^2/mL and were found not to be toxic to RAW264.7 cells at one hour (A-PS: $p = 0.85$ and U-PS: 0.82, Fig S5). Following 24 hours of incubation, the A-PS particles reduced cellular viability ($p < 0.05$ for concentrations ≥ 3.75 cm^2/mL) whereas no effect was observed for the U-PS particles ($p = 0.79$, Fig S5). The results of the dose response at 24 hours were verified with a clonogenic assay, which showed significant toxicity of the A-PS particles from a concentration of ≥ 0.23 cm^2/mL ($p < 0.05$, Fig S6) but not for the U-PS particles when compared to no NP particles present ($p = 0.34$, Fig S6).

A-PS particle association to macrophage-like RAW cells analysed by Coherent anti-Stokes Raman spectroscopy (CARS)

Imaging with coherent anti-Stokes Raman spectroscopy (CARS) was used to quantify the association of unlabelled A-PS particles to the murine macrophage-like RAW 264.7 cells. Some of the NPs were pre-incubated with SP-A (10 μg/mL) for an hour before incubating with the cells. Initial experiments showed that individual 100 nm NPs could not be resolved with enough specificity using this technique (data not shown). However, 200 nm A-PS particles were resolvable and therefore used in this study. The CARS analysis showed that SP-A inhibited the association of the A-PS NPs to the cells (**Fig 3A**). Quantification of the 200 nm A-PS particles compared to the area of the cells showed that SP-A significantly decreased the association of the A-PS NPs with the cells ($p = 0.029$**, Fig 3B**).

NP uptake into RAW cells and mouse alveolar macrophages analysed by FACS.

To examine the effect of SP-A interaction with 100 nm NPs specifically on cellular uptake, rather than just cellular association, we performed dose response experiments using a two-fold serial dilution of SP-A from 20 – 0 μg/mL with 100 nm fluorescent U-PS or A-PS NPs using the macrophage-like cell line RAW264.7 in the presence of calcium (**Fig. 4**). Following NP treatment and directly before FACS analysis the cells

were treated with trypan blue, which quenches the fluorescent signal outside the cells (Hartshorn et al., 1994). SP-A significantly increased the uptake of U-PS into the RAW cells at concentrations of ≥10 μg/mL ($p < 0.01$ with SP-A ≥10 μg/mL) whereas the uptake of A-PS was significantly reduced in the presence of SP-A at concentrations of ≥0.156 μg/mL ($p < 0.05$ at SP-A ≥ 0.156 μg/mL) compared to the absence of SP-A (**Fig 4**). Bovine serum albumin (BSA) was used as a non-specific protein control at a concentration of 20 μg/mL for both types of particles. BSA caused non-significant increases in the uptake of both U-PS particles (3.8% increase, $p = 0.44$) and A-PS particles (9.1% increase, $p = 0.19$) (data not shown).

The effect of SP-A on the uptake of A-PS and U-PS in the alveolar macrophages (AM) from wild type (WT) and SP-A knock-out mice (SP-$A^{-/-}$) was also examined. An increase in the uptake of 100 nm A-PS particles in AM from SP-$A^{-/-}$ mice was observed when compared to AM isolated from WT mice (**Fig 5A**). No statistically significant difference was seen when the uptake of 100 nm U-PS particles was compared in alveolar macrophages from SP-$A^{-/-}$ and WT mice (**Fig. 5A**). Furthermore, no statistically significant difference was seen in the uptake of either 500 nm U-PS or A-PS particles in SP-$A^{-/-}$ and WT alveolar macrophages (**Fig. 5A**). This suggests there might be a dependency on both the size and surface chemistry of the SP-A inhibition observed for the 100 nm A-PS particles. We next investigated the effect of exogenous SP-A on the uptake of 100 nm U-PS and A-PS particles into alveolar macrophages isolated from SP-$A^{-/-}$ and WT mice. The 100 nm particles were chosen for the SP-A add back experiments as no significant difference was observed in the uptake of either the 500 nm A-PS or 500 nm U-PS particles between WT and SP-$A^{-/-}$ mice. Consistent with the previous experiments there was a significant increase in the uptake of 100 nm A-PS particles in SP-$A^{-/-}$ macrophages compared to WT macrophages ($P < 0.002$) (**Fig 5B**). The pre-incubation of exogenous SP-A with A-PS particles decreased the uptake by alveolar macrophages from both groups of mice significantly compared to in the absence of SP-A ($p < 0.001$ for both mouse groups) (**Fig 5B**). An increase was seen in the uptake of 100 nm U-PS particles by the addition of SP-A to alveolar macrophages isolated from both groups of mice but this did not reach statistical significance (WT: $p = 0.26$ and SP-$A^{-/-}$: $p = 0.17$) (**Fig. 5C**).

Discussion

We have previously characterised the interaction between SP-D and PS particles with different surface modifications (Kendall et al., 2013). This showed that SP-D differentially interacts with particles, modifying their uptake by alveolar macrophages and lung-derived dendritic cells. The purpose of this study was to investigate whether SP-A showed differential interaction with PS nanoparticles with different surface charge and if this interaction affected uptake of these nanoparticles into macrophages in a similar or complementary way to SP-D.

Nanoparticle characterisation

The size of SP-A in water remained stable at around 30 nm, which is consistent with the literature, where human SP-A has previously been measured by DLS to be 42 ± 6 nm (López-Sánchez et al., 2011) and electron micrographs of recombinant human SP-A being less than 50 nm in length (Voss et al., 1988).

The incubation of U-PS particles with SP-A or BSA resulted in the zeta potentials of the particle suspensions moving closer to zero. This shows that the addition of protein to the particle suspension results in a reduction in colloidal stability, a process which enhances the likelihood of particle agglomeration. . This observation is similar to the findings by Ruge and colleagues, where they observed that SP-A and BSA had similar effects when incubated with magnetite nanoparticles with different surface charges (Ruge et al., 2011). In the current study SP-A changed the ZP for A-PS particles from a positive to a negative charge when incubated in TBS with calcium (+24.4 to -7.4 mV) or nanopure water (+60 to -22.8 mV). This is also similar to the findings by Ruge and colleagues when using particles with a positive zeta potential (Ruge et al., 2011).

Protein coronas which form around nanoparticles usually consist of an outer layer of loosely associated proteins termed the “soft” corona and an inner layer of strongly associated proteins called the “hard” corona (Deng et al., 2012, Barran-Berdon et al., 2013). Differences in particle agglomeration following incubation with SP-A may be linked to altered protein association with the particles. In particle association studies using SDS PAGE we found that SP-A formed a hard corona around U-PS but not A-PS particles (**Fig S4**). The changes in the DLS and zeta potential measurements suggests that SP-A forms a soft corona around the A-PS particles. This shows that differences in the particle surface chemistry can influence the interaction of SP-A with the particles, which in turn may influence particle agglomeration and uptake.

Furthermore, this study has shown that although SP-A mediated agglomeration of U-PS particles dependent on the presence of calcium, the association of SP-A with these particles is calcium independent. Although the zeta potential for both NPs bound by SP-A is around -20 mV in nanopure water and around -10 mV in TBS, the agglomeration kinetics are different. The U-PS particles agglomerated in the presence of SP-A whereas disagglomeration occurred for A-PS particles. This again implies a differential SP-A binding mechanism for these two types of particle. SP-A has been reported to self-agglomerate under certain conditions. Binding of SP-A to U-PS particles could facilitate conformational changes in SP-A that would enhance protein self-agglomeration or agglomeration of the U-PS particles. In the case of A-PS particles, the results indicate that the presence of the SP-A molecule at the particle surface may block the sites on the particle involved in self-agglomeration. SP-A would thereby inhibit A-PS self-agglomeration. The degree to which this is an SP-A specific effect is unclear as BSA also inhibits A-PS agglomeration. Further work examining the particle agglomeration kinetics following SP-A incubation is necessary using techniques that allow the accurate quantification of particle size in highly polydispersed suspensions.

SP-A mediated agglomeration of U-PS is dependent on calcium concentration

We found that a minimum concentration of 2 mM calcium was required for SP-A to agglomerate the 100 nm U-PS particles (**Fig S3**). This minimum calcium concentration is consistent with findings reported by Haagsman who observed that SP-A became saturated with calcium around a free calcium concentration of 2 mM (Haagsman et al., 1990). This also agrees with structural findings reported for the recombinant fragment of human SP-D, where this calcium concentration was thought to act like a molecular switch in the lectin binding site (Shrive et al., 2003). These findings indicate that the carbohydrate recognition domain (CRD) may be involved in the agglomeration of the U-PS particles. Calcium is required to stabilise the conformation of the lectin binding domain (Head et al., 2003). By using the structure of trimeric fragment of rat SP-A and computer modelling Head and colleagues showed that the electrostatic surface of the CRD of the SP-A becomes less negatively charged when calcium is present in the CRD (Head et al., 2003). The SP-A induced agglomeration of NPs might not directly involve the actual lectin binding site in the CRD region but the overall conformation or electrostatic surface charged induced by

calcium could result in a differential interaction than that seen in the absence of calcium. We have previously shown that a recombinant fragment of SP-D (rfhSP-D), containing a trimeric unit of neck and CRD regions only (**Fig S1**), is enough to interact with the particles used in this study (Kendall et al., 2013). It therefore seems plausible to extend this finding to SP-A. SP-A would, by crosslinking individual particles via individual trimeric units, be able to agglomerate NPs. These results also show that SP-A has a different interaction with surface modified NPs compared to native SP-D. SP-A inhibits the agglomeration of A-PS particles whereas SP-D facilitates A-PS particle agglomeration. Both SP-A and SP-D agglomerated U-PS particles in the presence of calcium (summarized in **Fig 6A**).

Nanoparticle toxicity

We show here that the used A-PS and U-PS particles were not toxic to the RAW 264.7 cells over short incubation periods such as those used in the *in vitro* cellular experiments (**Fig S5 and S6**). The observed difference between in the effect of SP-A on A-PS and U-PS particles is therefore not due to the toxicity of short term exposure of the cells with the NPs. However, when extending the incubation period from one hour to 24 hours the A-PS particles did show toxic effects on the cells while no toxic effect was observed for the U-PS particles. This is consistent with previous reports where it was observed that A-PS but not U-PS particles had a toxic effect on the TT1 cell line, a human alveolar epithelial type I like cell line (Ruenraroengsak et al., 2011). This highlights the difference between the "high dose - short exposure" acute toxicity models often used in *in vitro* assays and real life exposure scenarios where there is often low concentration of NPs but a long/chronic exposure period.

SP-A promotes or inhibits cellular uptake of NPs depending on the surface chemistry and size of particle.

Macrophage-like RAW264.7 cells were used to investigate the interactions of SP-A with NPs on phagocytic NP uptake. We found that SP-A enhanced the uptake of U-PS particles in a dose dependent manner, but inhibited the uptake of A-PS particles. To investigate this further we isolated alveolar macrophages from SP-$A^{-/-}$ mice, which would have no SP-A associated with them and compared them to alveolar macrophages from WT mice, that would have SP-A associated with them. SP-$A^{-/-}$ alveolar macrophages were not deficient in uptake of 100 nm or 500 nm U-PS or 500 nm A-PS particles compared to the control WT alveolar macrophages. However, there

was a significantly increased uptake of 100 nm A-PS into alveolar macrophages isolated from SP-A$^{-/-}$ mice compared to WT alveolar macrophages. The interaction was further confirmed by coating NPs with SP-A prior to incubation with alveolar macrophages isolated from SP-A$^{-/-}$ and WT mice, respectively, showing that SP-A inhibited the uptake of A-PS particles by cells from both groups of mice. The reduction of macrophage clearance of 100 nm A-PS particles following pre-incubation of SP-A could be mediated, at least in part, through the inhibition of A-PS self-agglomeration at physiological temperatures. However, BSA also showed the ability to inhibit A-PS agglomeration but had little effect on the uptake of A-PS particles by RAW cells. This finding coupled with the enhanced uptake of A-PS particles by AM from SP-A$^{-/-}$ mice suggests that mechanisms other than the inhibition of A-PS agglomeration may be involved in the SP-A mediated reduction of A-PS uptake. The reduction in phagocytic clearance of potentially toxic particles may result in enhanced exposure or damage to the alveolar epithelium and/ or increased translocation to extrapulmonary sites through the systemic circulation. We have previously shown that exogenous SP-D can enhance the uptake of 100 nm A-PS particles by alveolar macrophages from SP-D deficient mice (Kendall et al., 2013). It would therefore, be interesting to determine in future experiments whether the presence of SP-D could alter the ability of SP-A to inhibit the clearance of these particles by alveolar macrophages.

Potential impact in vivo

It is thought that NPs move by diffusion and pass through the trachea bronchiolar region into the alveoli, where they are deposited and may remain for some time (Muhlfeld et al., 2008). Once they enter the surfactant hypophase they have the opportunity to interact with surfactant lipids and proteins such as SP-A and SP-D (**Fig 6B**). Lipids and proteins absorb onto the particle surface forming coronas (Walkey et al., 2012). This bio-corona leads to changes in surface chemistry and colloidal stability (Ruge et al., 2012). The particles may be directly taken up by alveolar macrophages (Geiser et al., 2008, Erpenbeck et al., 2005). However, changes to surface chemistry could result in different pattern recognition by defence molecules or surface receptors on cells and could therefore potentially influence the fate of nanomaterials. As SP-A and SP-D show differential interaction with the particles used in this paper the two proteins could potentially complement each other *in vivo*.

It has been shown that both lipids and proteins from surfactant interact with nanoparticles (Kendall, 2007, Bakshi et al., 2008). In order to create a more realistic *in vitro* model of *in vivo* conditions, it would be beneficial to include lipids in these models for future experiments. Ruge and colleagues looked at SP-A and SP-D with metal-nanoparticles with different surface coatings and found differential effects of SP-A and SP-D (Ruge et al., 2012). They also observed that incorporating surfactant lipids into the *in vitro* models modified the effects of SP-A and SP-D (Ruge et al., 2012). This highlights the fact that current *in vitro* models do not reflect what happens *in vivo*. Human bronchoalveolar lavage can agglomerate nanoparticles (Kendall et al., 2002). An *in vitro* model using the natural porcine surfactant preparation Curosurf (devoid of SP-A and SP-D) also modified the effect of multi-walled carbon nanotubes and enhanced their oxidative and pro-inflammatory effects (Gasser et al., 2012). In order to have a comprehensive understanding of how nanoparticles interact with both surfactant proteins and lipids it is important to understand how NPs interact not only with specific subcomponents of surfactant but also implementing a model system that resembles *in vivo* circumstances as recently highlighted by Schleh and colleagues (Schleh et al., 2013).

Agglomeration seems to be the key to enhanced uptake into AMs in these observations and the surface chemistry described provides a mechanism for agglomeration by SP-A. However, SP-A provides important immune functions within the airspace and sequestering by NPs may leave an individual vulnerable to other pathogenic events and uncontrolled inflammation. We have previously shown that three different types of carbon black particles, ranging from 25-75 nm in diameter, were able to completely eliminate SP-D from a suspension (Kendall et al., 2004). Furthermore, an animal study exposing rats infected with *Streptococcus pneumoniae* to $PM_{2.5}$ particles resulted in an exacerbation of the on-going infection (Zelikoff et al., 2003). We have recently shown that incubating these nanoparticles with SP-A and SP-D alters the ability of these proteins to neutralise influenza A infection *in vitro* (McKenzie et al., 2014). This implies that sequestering immune related proteins could result in functionally deficient individuals resulting in an increase in their susceptibility towards bacterial and viral infections and other inflammatory conditions as observed in mice deficient for SP-A or SP-D (Hawgood et al., 2004, Li et al., 2002, LeVine and Whitsett, 2001). It is therefore important that more research is performed to elucidate the implications of the interactions between surfactant protein A and D

and NPs in order to evaluate the potential health implications when implementing the usage of NPs in the working environment and everyday modern consumer products.

Conclusions

Here we have characterised the interaction between NPs and SP-A, examined the effect on cellular uptake, and propose uptake mechanics into macrophages. SP-A showed material specific binding and calcium dependent agglomeration of U-PS nanoparticles. We showed that SP-A inhibited the uptake of 100 nm A-PS nanoparticles into macrophage-like cells and primary alveolar macrophages using CARS (unlabelled 200 nm NPs) and FACS (fluorescent NPs) but this was not observed for larger (500 nm) A-PS particles.

This study combined with previous studies with SP-A and SP-D shows that these molecules may have a (complementary) role in clearing non-pathogen particulate and nanoparticulate materials *in vivo*. An important factor, when examining the interaction of SP-A or SP-D with NPs, is to consider how the interplay between surfactant lipids and proteins in the bio-corona will affect the interaction and the subsequent downstream bioavailability of the collectins. Future *in vivo* studies focusing on the interaction between these lung collectins, NPs and the clearance route(s) into cells and body compartments is required to provide further insight into the role(s) of SP-A and SP-D in response to inhalation of NPs.

Acknowledgement

This work was funded under the Joint Environment and Human Health programme (NERC-EPSRC Project NEE009395-1), funded by agencies of the UK Government: The Natural Environment Research Council (NERC), Department for Environment Food and Rural Affairs (Defra), Environment Agency (EA), Ministry of Defence (MOD) and the Medical Research Council (MRC). We gratefully acknowledge the financial support of the MRC ITTP Toxicology Unit for Z McKenzie. The use of FENAC (Facility for Environmental Nanoscience Analysis and Characterisation) was supported by NERC FENAC access grant 2013/05/004. This work was also supported by the National Institute of Health Research (NIHR) funded Respiratory Biomedical Research Units of University Hospital Southampton and the Royal Brompton and Harefield NHS Foundation Trust. SM acknowledges EPSRC Laser Loan Pool support, which enabled the CARS experiments.

MK, HWC and JM developed the concepts in all the detailed experiments. MK, HWC and JM wrote and managed the proposal outlining the experimental design. MG and CM organised and collected the human BAL. ZM, HW, CE and PD prepared the materials and conducted DLS. ZM, MK, HW, CE and PD jointly interpreted and synthesised the protein-NP data to form conclusions. ZM, RM, HWC and JM designed the RAW264.7 and alveolar macrophage experiments. ZM and RM conducted the RAW264.7 and alveolar macrophage experiments. SM performed the CARS experiments and the analysis ZM, MK RM, HWC and JM jointly interpreted and synthesised the cell data to form the protein-NP manuscript. ZM, MK, RM, HW, CE, PD, MG, CM, SM, HWC and JM jointly revised the manuscript critically for important intellectual content.

We thank Dr Tony Willis for the N-terminal sequencing of purified native human SP-A.

Declaration of interest

The authors do not have any competing financial interests with the work in this article.

References

BAKSHI, M. S., ZHAO, L., SMITH, R., POSSMAYER, F. & PETERSEN, N. O. 2008. Metal nanoparticle pollutants interfere with pulmonary surfactant function in vitro. *Biophys J,* 94**,** 855-68.

BARRAN-BERDON, A. L., POZZI, D., CARACCIOLO, G., CAPRIOTTI, A. L., CARUSO, G., CAVALIERE, C., RICCIOLI, A., PALCHETTI, S. & LAGANA, A. 2013. Time evolution of nanoparticle-protein corona in human plasma: relevance for targeted drug delivery. *Langmuir,* 29**,** 6485-94.

BORRON, P., MCINTOSH, J. C., KORFHAGEN, T. R., WHITSETT, J. A., TAYLOR, J. & WRIGHT, J. R. 2000. Surfactant-associated protein A inhibits LPS-induced cytokine and nitric oxide production in vivo. *Am J Physiol Lung Cell Mol Physiol,* 278**,** L840-7.

BORRON, P., VELDHUIZEN, R. A., LEWIS, J. F., POSSMAYER, F., CAVENEY, A., INCHLEY, K., MCFADDEN, R. G. & FRAHER, L. J. 1996. Surfactant associated protein-A inhibits human lymphocyte proliferation and IL-2 production. *Am J Respir Cell Mol Biol,* 15**,** 115-21.

BORRON, P. J., CROUCH, E. C., LEWIS, J. F., WRIGHT, J. R., POSSMAYER, F. & FRAHER, L. J. 1998. Recombinant rat surfactant-associated protein D inhibits human T lymphocyte proliferation and IL-2 production. *J Immunol,* 161**,** 4599-603.

BRINKER, K. G., GARNER, H. & WRIGHT, J. R. 2003. Surfactant protein A modulates the differentiation of murine bone marrow-derived dendritic cells. *Am J Physiol Lung Cell Mol Physiol,* 284**,** L232-41.

CLARK, H., PALANIYAR, N., STRONG, P., EDMONDSON, J., HAWGOOD, S. & REID, K. B. 2002. Surfactant protein D reduces alveolar macrophage apoptosis in vivo. *J Immunol,* 169**,** 2892-9.

DENG, Z. J., LIANG, M., TOTH, I., MONTEIRO, M. J. & MINCHIN, R. F. 2012. Molecular interaction of poly(acrylic acid) gold nanoparticles with human fibrinogen. *ACS Nano,* 6**,** 8962-9.

ERPENBECK, V. J., MALHERBE, D. C., SOMMER, S., SCHMIEDL, A., STEINHILBER, W., GHIO, A. J., KRUG, N., WRIGHT, J. R. & HOHLFELD, J. M. 2005. Surfactant protein D increases phagocytosis and aggregation of pollen-allergen starch granules. *Am J Physiol Lung Cell Mol Physiol,* 288**,** L692-8.

GASSER, M., WICK, P., CLIFT, M. J., BLANK, F., DIENER, L., YAN, B., GEHR, P., KRUG, H. F. & ROTHEN-RUTISHAUSER, B. 2012. Pulmonary surfactant coating of multi-walled carbon nanotubes (MWCNTs) influences their oxidative and pro-inflammatory potential in vitro. *Part Fibre Toxicol,* 9**,** 17.

GEISER, M., CASAULTA, M., KUPFERSCHMID, B., SCHULZ, H., SEMMLER-BEHNKE, M. & KREYLING, W. 2008. The role of macrophages in the clearance of inhaled ultrafine titanium dioxide particles. *Am J Respir Cell Mol Biol,* 38**,** 371-6.

HAAGSMAN, H. P., SARGEANT, T., HAUSCHKA, P. V., BENSON, B. J. & HAWGOOD, S. 1990. Binding of calcium to SP-A, a surfactant-associated protein. *Biochemistry,* 29**,** 8894-900.

HANSEN, S., LO, B., EVANS, K., NEOPHYTOU, P., HOLMSKOV, U. & WRIGHT, J. R. 2007. Surfactant protein D augments bacterial association but attenuates major histocompatibility complex class II presentation of bacterial antigens. *Am J Respir Cell Mol Biol,* 36**,** 94-102.

HARTSHORN, K. L., CROUCH, E. C., WHITE, M. R., EGGLETON, P., TAUBER, A. I., CHANG, D. & SASTRY, K. 1994. Evidence for a protective role of pulmonary surfactant protein D (SP-D) against influenza A viruses. *J Clin Invest,* 94**,** 311-9.

HAWGOOD, S., BROWN, C., EDMONDSON, J., STUMBAUGH, A., ALLEN, L., GOERKE, J., CLARK, H. & POULAIN, F. 2004. Pulmonary collectins modulate strain-specific influenza a virus infection and host responses. *J Virol,* 78**,** 8565-72.

HEAD, J. F., MEALY, T. R., MCCORMACK, F. X. & SEATON, B. A. 2003. Crystal structure of trimeric carbohydrate recognition and neck domains of surfactant protein A. *J Biol Chem,* 278**,** 43254-60.

KENDALL, M. 2007. Fine airborne urban particles (PM2.5) sequester lung surfactant and amino acids from human lung lavage. *Am J Physiol Lung Cell Mol Physiol,* 293**,** L1053-8.

KENDALL, M., BROWN, L. & TROUGHT, K. 2004. Molecular adsorption at particle surfaces: a PM toxicity mediation mechanism. *Inhal Toxicol,* 16 Suppl 1**,** 99-105.

KENDALL, M., DING, P., MACKAY, R. M., DEB, R., MCKENZIE, Z., KENDALL, K., MADSEN, J. & CLARK, H. 2013. Surfactant protein D (SP-D) alters cellular uptake of particles and nanoparticles. *Nanotoxicology,* 7**,** 963-73.

KENDALL, M. & HOLGATE, S. 2012. Health impact and toxicological effects of nanomaterials in the lung. *Respirology,* 17**,** 743-58.

KENDALL, M., TETLEY, T. D., WIGZELL, E., HUTTON, B., NIEUWENHUIJSEN, M. & LUCKHAM, P. 2002. Lung lining liquid modifies PM(2.5) in favor of particle aggregation: a protective mechanism. *Am J Physiol Lung Cell Mol Physiol,* 282**,** L109-14.

LEVINE, A. M., BRUNO, M. D., HUELSMAN, K. M., ROSS, G. F., WHITSETT, J. A. & KORFHAGEN, T. R. 1997. Surfactant protein A-deficient mice are susceptible to group B streptococcal infection. *J Immunol,* 158**,** 4336-40.

LEVINE, A. M., GWOZDZ, J., STARK, J., BRUNO, M., WHITSETT, J. & KORFHAGEN, T. 1999a. Surfactant protein-A enhances respiratory syncytial virus clearance in vivo. *J Clin Invest,* 103**,** 1015-21.

LEVINE, A. M., HARTSHORN, K., ELLIOTT, J., WHITSETT, J. & KORFHAGEN, T. 2002. Absence of SP-A modulates innate and adaptive defense responses to pulmonary influenza infection. *Am J Physiol Lung Cell Mol Physiol,* 282**,** L563-72.

LEVINE, A. M., KURAK, K. E., BRUNO, M. D., STARK, J. M., WHITSETT, J. A. & KORFHAGEN, T. R. 1998. Surfactant protein-A-deficient mice are susceptible to Pseudomonas aeruginosa infection. *Am J Respir Cell Mol Biol,* 19**,** 700-8.

LEVINE, A. M., KURAK, K. E., WRIGHT, J. R., WATFORD, W. T., BRUNO, M. D., ROSS, G. F., WHITSETT, J. A. & KORFHAGEN, T. R. 1999b. Surfactant protein-A binds group B streptococcus enhancing phagocytosis and clearance from lungs of surfactant protein-A-deficient mice. *Am J Respir Cell Mol Biol,* 20**,** 279-86.

LEVINE, A. M. & WHITSETT, J. A. 2001. Pulmonary collectins and innate host defense of the lung. *Microbes Infect,* 3**,** 161-6.

LI, G., SIDDIQUI, J., HENDRY, M., AKIYAMA, J., EDMONDSON, J., BROWN, C., ALLEN, L., LEVITT, S., POULAIN, F. & HAWGOOD, S. 2002. Surfactant protein-A--deficient mice display an exaggerated early

inflammatory response to a beta-resistant strain of influenza A virus. *Am J Respir Cell Mol Biol,* 26**,** 277-82.
LÓPEZ-SÁNCHEZ, A., SÁENZ, A. & CASALS, C. 2011. Surfactant protein A (SP-A)-tacrolimus complexes have a greater anti-inflammatory effect than either SP-A or tacrolimus alone on human macrophage-like U937 cells. *Eur J Pharm Biopharm,* 77**,** 384-91.
MCKENZIE, Z., KENDALL, M., MACKAY, R.-M., TETLEY, T., MORGAN, C., MARK, G., CLARK, H. & MADSEN, J. 2014. Nanoparticles modulate Surfactant Protein A and D mediated protection against Influenza A infection *in vitro*. *Philosophical Transactions of the Royal Society B Biological Sciences,* Manuscript in press.
MUHLFELD, C., ROTHEN-RUTISHAUSER, B., BLANK, F., VANHECKE, D., OCHS, M. & GEHR, P. 2008. Interactions of nanoparticles with pulmonary structures and cellular responses. *Am J Physiol Lung Cell Mol Physiol,* 294**,** L817-29.
NANOTECHNOLOGIES, T. P. O. E. 2014. *Consumer Products Inventory* [Online]. Nanotechnology. Available: http://www.nanotechproject.org/cpi/ [Accessed 9 September 2014].
OBERDORSTER, G., MAYNARD, A., DONALDSON, K., CASTRANOVA, V., FITZPATRICK, J., AUSMAN, K., CARTER, J., KARN, B., KREYLING, W., LAI, D., OLIN, S., MONTEIRO-RIVIERE, N., WARHEIT, D. & YANG, H. 2005. Principles for characterizing the potential human health effects from exposure to nanomaterials: elements of a screening strategy. *Part Fibre Toxicol,* 2**,** 8.
OBERDÖRSTER, G., OBERDÖRSTER, E. & OBERDÖRSTER, J. 2005. Nanotoxicology: an emerging discipline evolving from studies of ultrafine particles. *Environ Health Perspect,* 113**,** 823-39.
OBERDORSTER, G., SHARP, Z., ATUDOREI, V., ELDER, A., GELEIN, R., LUNTS, A., KREYLING, W. & COX, C. 2002. Extrapulmonary translocation of ultrafine carbon particles following whole-body inhalation exposure of rats. *Journal of Toxicology and Environmental Health-Part A,* 65**,** 1531-1543.
PALANIYAR, N., CLARK, H., NADESALINGAM, J., HAWGOOD, S. & REID, K. B. 2003. Surfactant protein D binds genomic DNA and apoptotic cells, and enhances their clearance, in vivo. *Ann N Y Acad Sci,* 1010**,** 471-5.
PASTVA, A. M., WRIGHT, J. R. & WILLIAMS, K. L. 2007. Immunomodulatory roles of surfactant proteins A and D: implications in lung disease. *Proc Am Thorac Soc,* 4**,** 252-7.
PATEL, I. I., STEUWE, C., REICHELT, S. & MAHAJAN, S. 2013. Coherent anti-Stokes Raman scattering for label-free biomedical imaging. *Journal of Optics,* 15.
PÉREZ-GIL, J. 2008. Structure of pulmonary surfactant membranes and films: the role of proteins and lipid-protein interactions. *Biochim Biophys Acta,* 1778**,** 1676-95.
RASCHKE, W. C., BAIRD, S., RALPH, P. & NAKOINZ, I. 1978. Functional macrophage cell lines transformed by Abelson leukemia virus. *Cell,* 15**,** 261-7.
RUENRAROENGSAK, P., NOVAK, P., BERHANU, D., THORLEY, A. J., VALSAMI-JONES, E., GORELIK, J., KORCHEV, Y. E. & TETLEY, T. D. 2011. Respiratory epithelial cytotoxicity and membrane damage (holes) caused by amine-modified nanoparticles. *Nanotoxicology*.

RUGE, C. A., KIRCH, J., CANADAS, O., SCHNEIDER, M., PEREZ-GIL, J., SCHAEFER, U. F., CASALS, C. & LEHR, C. M. 2011. Uptake of nanoparticles by alveolar macrophages is triggered by surfactant protein A. *Nanomedicine,* 7**,** 690-3.

RUGE, C. A., SCHAEFER, U. F., HERRMANN, J., KIRCH, J., CANADAS, O., ECHAIDE, M., PEREZ-GIL, J., CASALS, C., MULLER, R. & LEHR, C. M. 2012. The interplay of lung surfactant proteins and lipids assimilates the macrophage clearance of nanoparticles. *PLoS One,* 7**,** e40775.

SALVADOR-MORALES, C., TOWNSEND, P., FLAHAUT, E., VE´NIEN-BRYAN, C., VLANDAS, A., GREEN, M. L. H. & SIM, R. B. 2007. Binding of pulmonary surfactant proteins to carbon nanotubes; potential for damage to lung immune defense mechanisms. *Carbon,* 45**,** 607 - 617.

SCHLEH, C., KREYLING, W. G. & LEHR, C. M. 2013. Pulmonary surfactant is indispensable in order to simulate the in vivo situation. *Part Fibre Toxicol,* 10**,** 6.

SCHULZE, C., SCHAEFER, U. F., RUGE, C. A., WOHLLEBEN, W. & LEHR, C. M. 2011. Interaction of metal oxide nanoparticles with lung surfactant protein A. *Eur J Pharm Biopharm,* 77**,** 376-83.

SHRIVE, A. K., THARIA, H. A., STRONG, P., KISHORE, U., BURNS, I., RIZKALLAH, P. J., REID, K. B. & GREENHOUGH, T. J. 2003. High-resolution structural insights into ligand binding and immune cell recognition by human lung surfactant protein D. *J Mol Biol,* 331**,** 509-23.

SUWABE, A., MASON, R. J. & VOELKER, D. R. 1996. Calcium dependent association of surfactant protein A with pulmonary surfactant: application to simple surfactant protein A purification. *Arch Biochem Biophys,* 327**,** 285-91.

VOSS, T., EISTETTER, H., SCHAFER, K. P. & ENGEL, J. 1988. Macromolecular organization of natural and recombinant lung surfactant protein SP 28-36. Structural homology with the complement factor C1q. *J Mol Biol,* 201**,** 219-27.

WALKEY, C. D., OLSEN, J. B., GUO, H., EMILI, A. & CHAN, W. C. 2012. Nanoparticle size and surface chemistry determine serum protein adsorption and macrophage uptake. *J Am Chem Soc,* 134**,** 2139-47.

WRIGHT, J. R., WAGER, R. E., HAWGOOD, S., DOBBS, L. & CLEMENTS, J. A. 1987. Surfactant apoprotein Mr = 26,000-36,000 enhances uptake of liposomes by type II cells. *J Biol Chem,* 262**,** 2888-94.

ZELIKOFF, J. T., CHEN, L. C., COHEN, M. D., FANG, K., GORDON, T., LI, Y., NADZIEJKO, C. & SCHLESINGER, R. B. 2003. Effects of inhaled ambient particulate matter on pulmonary antimicrobial immune defense. *Inhal Toxicol,* 15**,** 131-50.

Figure captions

Figure 1: **Dynamic Light Scattering analysis of the size distributions of 100 nm A-PS and U-PS particles in TBS/RPMI.** Size distributions of 100 nm A-PS (**A and B**) and 100 nm U-PS **(C and D**) nanoparticles in TBS-RPMI. 12.5 cm^2/mL of particles in TBS with 5 mM Ca^{2+} were mixed with 50 µg/mL BSA (■) or 50 µg/mL SP-A (▲) or TBS only (●) for 1 hour before being mixed with RPMI (TBS:RPMI; 2:3) and their size distributions immediately measured at 37^oC (**A and C**, T60) and again 2 hours later (**B and D**, T180). The final protein concentration was 10 µg/mL and nanoparticle concentrations were 2.5 cm^2/mL. Size distributions of nanoparticles in TBS only at T-2 are shown as dashed line.

Figure 2. Effect of SP-A on A-PS and U-PS particle agglomeration. The effect of SP-A (10 µg/mL) in the presence and absence of calcium (2 mM) in PBS on the agglomeration of 100 nm fluorescent orange-labelled A-PS or 100 nm fluorescent green-labelled U-PS particles (3.8 cm^2/mL) was evaluated using fluorescence microscopy. A-PS and U-PS particles were incubated with or without proteins for 1 hour at 37°C before being mounted onto slides for microscopy. Pictures were taken at x400 magnification.

Figure 3. The association of 200 nm unlabelled A-PS with (w) and without (w/o) SP-A to macrophage-like RAW264.7 cells visualised and quantified by CARS. A) CARS images. 200 nm A-PS particles show up as white particles (arrows). Note that other $–CH_2$ rich structures, such as the nuclear membrane, shows up as a visible ring in each cell (asterisks). **B**) CARS images were analysed using MATLAB software as described in the materials and methods section. N = 4 per column. Shown is the mean +/- standard derivation. $p < 0.05$ was considered statistically significant.

Figure 4. The effect of exogenous SP-A on the uptake of 100 nm A-PS and U-PS particles in macrophage-like RAW264.7 cells. Two-fold serial dilution of SP-A was incubated with fluorescent 100 nm A-PS or U-PS particles (3.8 cm2/mL) in the presence of calcium before incubating with RAW cells. Extra cellular association of NPs with cells were quenched using trypan blue. The particle uptake was analysed

using FACS. Shown are the mean +/- standard derivation of four independent experiments. * $p < 0.05$ and **** $p < 0.0001$.

Figure 5. Uptake of U-PS and A-PS and the effects of 10 µg/mL SP-A on the uptake by alveolar macrophages isolated from wild-type and SP-A$^{-/-}$ mice.
A) Uptake of FITC labelled 100 and 500 nm U-PS and A-PS particles (5:1 NP/cell) by AMs isolated from wild type mice (light grey) and SP-A$^{-/-}$ mice (dark grey). **B)** Fluorescent orange-labelled 100 nm A-PS (3.8 cm^2/mL) in the absence (light grey) of presence (dark grey) of SP-A with AMs from wild type mice and SP-A$^{-/-}$ mice. **C**) Fluorescent green-labelled 100 nm U-PS (3.8 cm^2/mL) in the absence (light grey) or presence (dark grey) of SP-A with AMs from wild type mice and SP-A$^{-/-}$ mice. The statistical analysis was determined using unpaired t-test as described in the materials and method section. $P < 0.05$ was considered statistical significant and significant values are shown in the figure. Data show relative mean fluorescence intensity (MFI) +/- standard derivation derived from 3 (Fig 5A and B) and 2 (Fig 5C) independent experiments with n = 3 mice per experiment.

Figure 6. The role of collectins in agglomeration of NPs. A) Differential interaction of SP-A, SP-D and rfhSP-D with 100 nm U-PS and A-PS particles.
Both SP-A and SP-D agglomerates U-PS particles in the presence of calcium. A-PS particles tend to self-agglomerates at 37^{o}C but SP-A inhibits that by binding to the particles whereas SP-D facilitates further agglomeration. The rfhSP-D binds to both A-PS and U-PS particles but does not facilitate agglomeration of the particles as seen with native SP-D (Kendall et al., 2013). The NPs, SP-A, SP-D and rfhSP-D are approximately to scale. **B) Simplistic model showing the roles of SP-A and SP-D and NP clearance *in vivo* in the alveolar space**. Inhaled particles enter the alveolar space (1) and deposit onto the air-liquid interface of the alveolus (2). The particles are then displaced into the fluid phase through wetting forces, resulting in the formation of a lipid biocorona (3). The biocorona is then modified through the incorporation of surfactant proteins, potentially resulting in particle agglomeration dependent on the surface chemistry of the particle (4). Particle agglomerates are recognised by alveolar macrophages (5) and phagocytosed (6). Abbreviations: ATI; alveolar epithelial type I cells, ATII alveolar epithelial type II cells. Model not to scale.

Table 1. Hydrodynamic size and zeta potential of A-PS and U-PS particles following incubation with SP-A or BSA. Z average (Z-AVE), polydispersity index (PDI) and zeta potential (ZP) of polystyrene particles incubated at 37°C at various time points (T-2 to T180). T-2 represents time point immediately prior to mixing with protein which occurred at T0. Particles – protein suspensions were then incubated for 48 mins at 37°C (T48) before the addition of serum free RPMI cell culture medium (T60). The particles were then incubated for a further 2 hours (T180). *$\Delta d = (d(t)-d(t-2))/d(t-2)$. The zeta potential of SP-A in TBS was -10.9 mV at T-2.

Table 1

NP	Media (Time point, mins)	Control				SP-A				BSA			
		Z-AVE (d, nm)	**Δd* (%)**	**PDI**	**ZP (mV)**	**Z-AVE (d, nm)**	**Δd* (%)**	**PDI**	**ZP (mV)**	**Z-AVE (d, nm)**	**Δd* (%)**	**PDI**	**ZP (mV)**
A-PS	TBS (T-2)	**109.7**	-	0.123	+24.4	**109.7**	-	0.123	+24.4	**109.7**	-	0.123	+24.4
	TBS (T0)	**258.8**	135.9	0.426	+14.9	**400.4**	265.0	0.465	-7.4	**392.3**	257.6	0.197	-3.3
	TBS (T48)	**1264**	1052.2	0.283	+15.7	**566.8**	416.7	0.429	-8.1	**579.2**	428.0	0.272	-4.1
	TBS + RPMI (T60)	**1693**	1443.3	0.340	-12.4	**573.7**	423.0	0.664	-9.3	**606.0**	452.4	0.218	-8.0
	TBS + RPMI (T180)	**2229**	1931.9	0.363	-9.3	**1142**	941.0	0.518	-12.4	**720.1**	556.4	0.376	-10.3
U-PS	TBS (T-2)	**127.6**	-	0.008	-26.8	**127.6**	-	0.008	-26.8	**127.6**	-	0.008	-26.8
	TBS (T0)	**136.5**	7.0	0.040	-26.1	**545.6**	327.6	0.363	-7.0	**148.8**	16.6	0.055	-8.7
	TBS (T48)	**151.1**	18.4	0.100	-17.0	**2224.0**	1642.9	0.328	-9.2	**134.2**	5.2	0.027	-8.3
	TBS + RPMI (T60)	**324.2**	154.1	0.262	-11.3	**1830.0**	1334.2	0.229	-9.4	**153.9**	20.6	0.064	-10.3
	TBS + RPMI (T180)	**1037.0**	712.7	0.540	-7.5	**2038.0**	1497.2	0.270	-9.2	**235.4**	84.5	0.441	-9.4

Figure 1

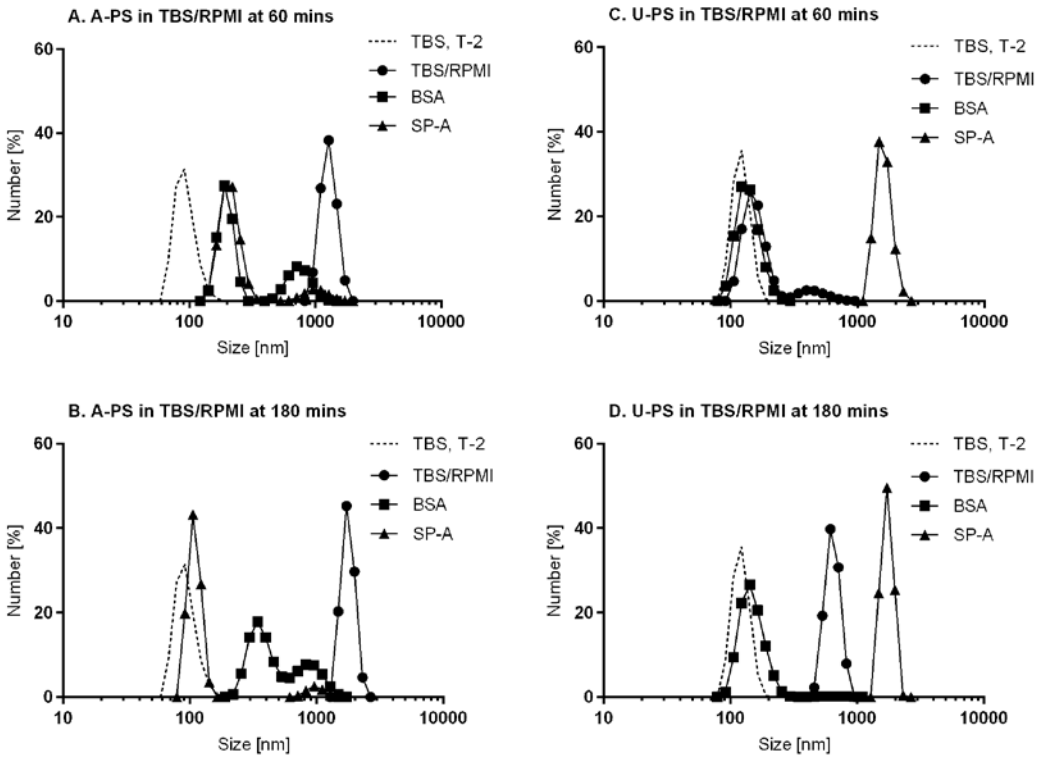
A. A-PS in TBS/RPMI at 60 mins
C. U-PS in TBS/RPMI at 60 mins
B. A-PS in TBS/RPMI at 180 mins
D. U-PS in TBS/RPMI at 180 mins
TBS, T-2
TBS/RPMI
BSA
SP-A
Number [%]
Size [nm]
0
20
40
60
10
100
1000
10000

Figure 2

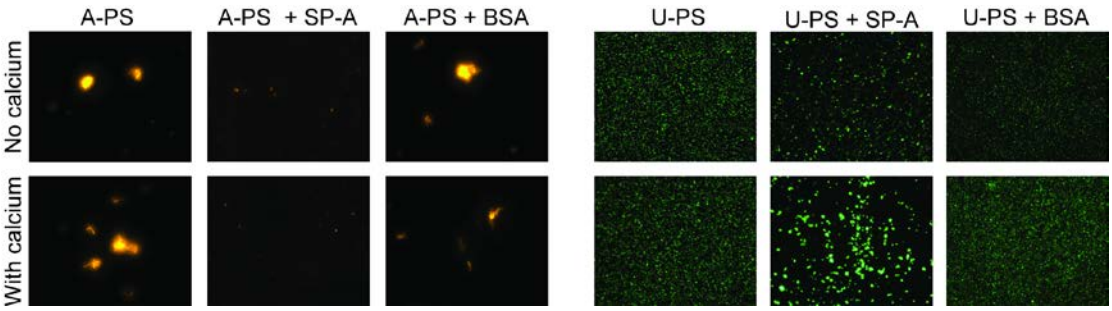
A-PS
A-PS + SP-A
A-PS + BSA
U-PS
U-PS + SP-A
U-PS + BSA
No calcium
With calcium

Figure 3

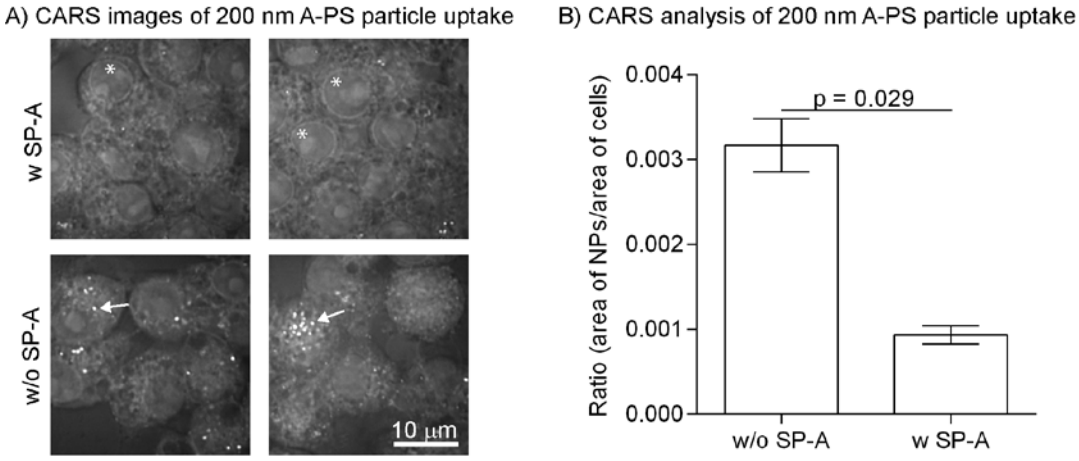
A) CARS images of 200 nm A-PS particle uptake
w SP-A
w/o SP-A
10 μm
B) CARS analysis of 200 nm A-PS particle uptake
Ratio (area of NPs/area of cells)
0.004
0.003
0.002
0.001
0.000
p = 0.029
w/o SP-A
w SP-A

Figure 4

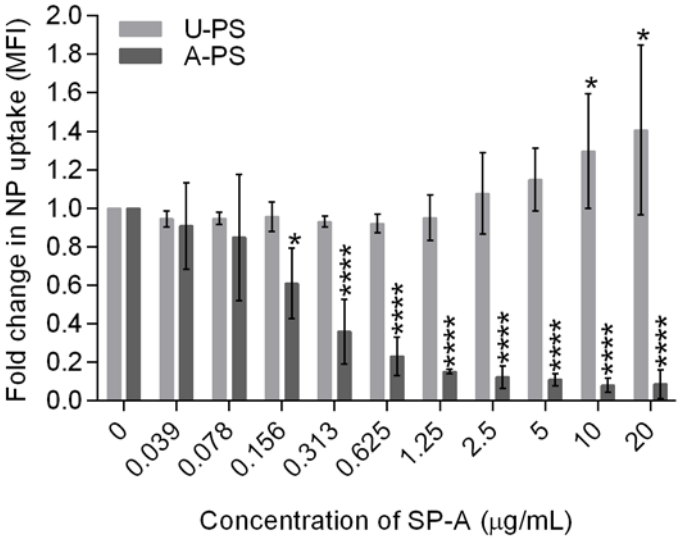
U-PS
A-PS
Fold change in NP uptake (MFI)
2.0
1.8
1.6
1.4
1.2
1.0
0.8
0.6
0.4
0.2
0.0
*
****
****
****
****
*
*
0
0.039
0.078
0.156
0.313
0.625
1.25
2.5
5
10
20
Concentration of SP-A (μg/mL)

Figure 5

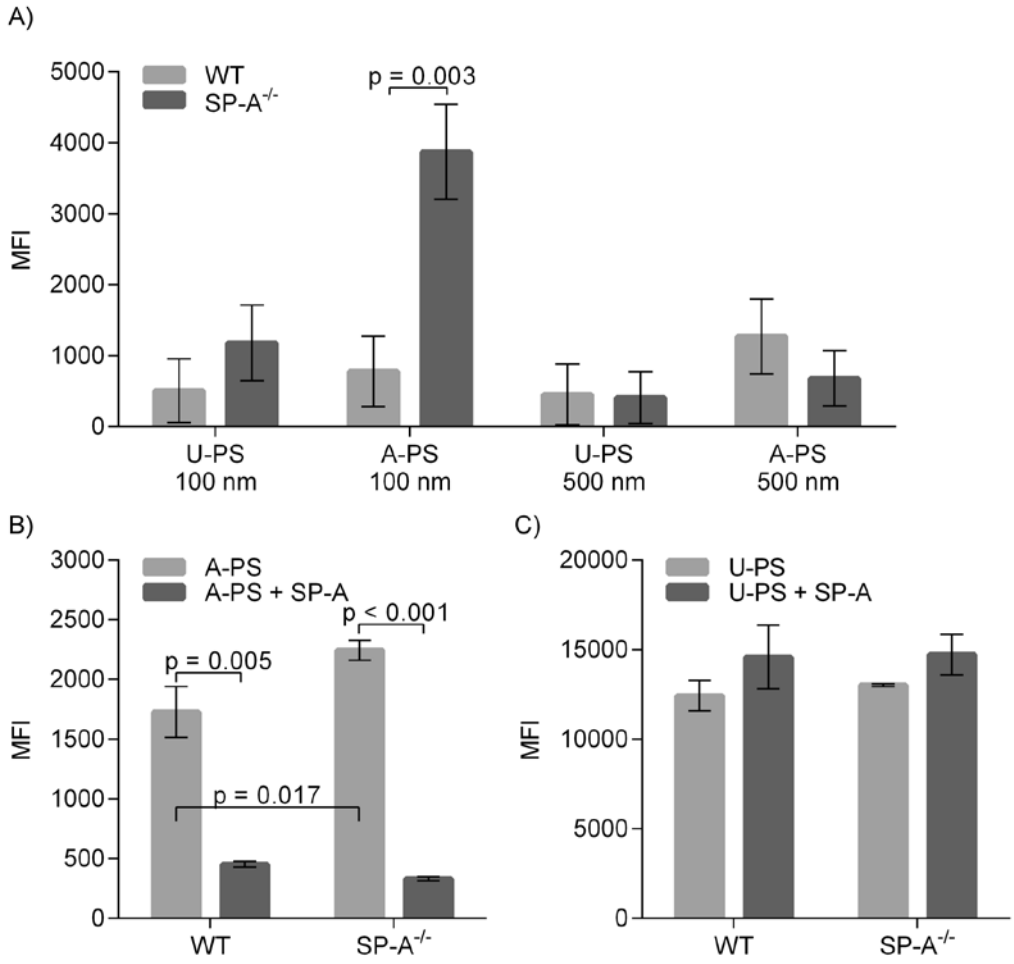
A)
WT
SP-A-/-
p = 0.003
MFI
5000
4000
3000
2000
1000
0
U-PS 100 nm
A-PS 100 nm
U-PS 500 nm
A-PS 500 nm
B)
A-PS
A-PS + SP-A
p = 0.005
p < 0.001
p = 0.017
MFI
3000
2500
2000
1500
1000
500
0
WT
SP-A-/-
C)
U-PS
U-PS + SP-A
MFI
20000
15000
10000
5000
0
WT
SP-A-/-

Figure 6

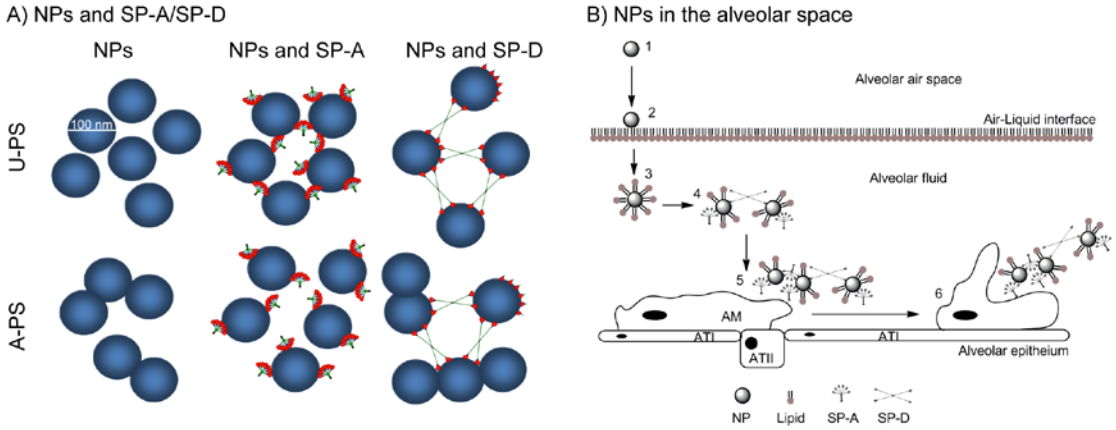
A) NPs and SP-A/SP-D
NPs
NPs and SP-A
NPs and SP-D
U-PS
A-PS
100 nm
B) NPs in the alveolar space
1
2
3
4
5
6
Alveolar air space
Air-Liquid interface
Alveolar fluid
AM
ATI
ATII
ATI
Alveolar epitheium
NP
Lipid
SP-A
SP-D

Supplementary figure captions

Figure S1. Human lung collectins and the recombinant fragment of human SP-D (rfhSP-D). A) Oligomerisation of SP-A and SP-D**.** Black: N-terminal region involved in the higher oligomerization of SP-A and SP-D; green: Collagenous region; blue: Neck region where trimerization of the three polypeptides initiates; orange: Carbohydrate recognition (lectin) domain (CRD). **B)** The trimeric recombinant fragment of human SP-D consisting of the 8 Gly-Xaa-Yaa repeats of the collagenous region, the neck region and the CRD region of native SP-D (Hakansson et al. 1999). Ribbon diagram generated with Chimera (Pettersen et al. 2004) from 1PW9 PDB file. Only the neck and CRD regions are shown in the ribbon diagram. Green spheres show the location of the calcium ions and the lectin binding sites in the CRDs.

Figure S2. Size distributions of SP-A by light intensity and number.
10 μg/mL SP-A in nanopure water. Size distribution based on light intensity (•) and number (○).

Figure S3. Effect of calcium on the size distributions of 100 nm U-PS and SP-A suspensions in water over time. A) U-PS particles (2.5 cm^2/mL) mixed with SP-A (10 μg/mL) in water without calcium. Mixing time: (●) 0 min, (○) 10 min, (▼) 240 min, (Δ) 1444 min. **B)** The effect of the calcium concentration on the relative size distributions after mixing U-PS particles (2.5 cm^2/mL) with SP-A (10 μg/mL); calcium concentrations: (•) 0 mM, (○) 0.2 mM, (▼) 1.0 mM, (Δ) 2.0 mM. **C)** Size distributions after mixing U-PS particles (2.5 cm^2/mL) with 10 μg/mL SP-A in the presence of 2 mM $CaCl_2$ over time (•) 0 min, (○) 10 min (▼) 30 min, (Δ) 120 min.

Figure S4. Reduced SDS-PAGE analysis of SP-A bound to 100 nm PS particles. Particles were incubated with SP-A for 24 hours at 37°C in TBS containing calcium or EDTA. The particles were then centrifuged and washed twice in the appropriate buffer (i.e. TBS containing Ca or EDTA) and the pellet examined using reduced SDS-PAGE analysis. The proteins were visualized using SimpleBlue SafeStain according to manufacture's protocol (LifeTechnologies, Paisley, UK)

Figure S5. Cell viability (MTT assay) of macrophage-like RAW264.7 cells following incubation with fluorescently labelled 100 nm A-PS or 100 nm U-PS particles. A) 1 hour incubation and **B**) 24 hours incubation. Data represents mean of three independent experiments +/- SEM conducted in triplicate. Statistics determined using ANOVA with LSD post hoc compared to nanoparticle free control. *p = 0.040, **p = 0.005, *** p < 0.001; 1 hour A-PS p = 0.85 (ANOVA); 1 hour U-PS p = 0.82 (ANOVA); 24 hours U-PS p = 0.79 (ANOVA).

Figure S6. Clonogenic survival of macrophage-like RAW264.7 cells following 24 hours incubation with fluorescently labelled 100 nm A-PS or 100 nm U-PS particles. Data represents mean of at least three independent experiments +/- SEM. Statistics determined using ANOVA with LSD post hoc test comparing against nanoparticle free control; *p = 0.020; ***p < 0.001.

Table S1. Size (intensity) and zeta potential of particles (2.5 cm^2/mL) before and after mixing with 10 µg/mL SP-A in water, Δd = (d(t)/d(t=0)). The zeta potential of 10 µg/mL SP-A alone was -11.8mV.

Figure S1

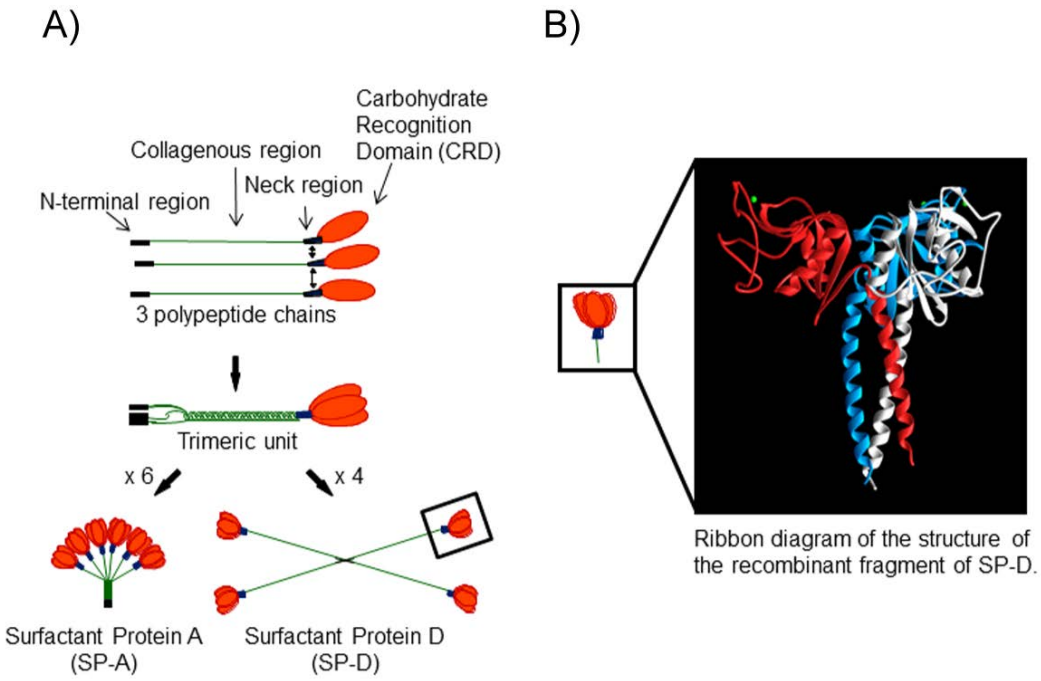
A)
B)
Carbohydrate Recognition Domain (CRD)
Collagenous region
Neck region
N-terminal region
3 polypeptide chains
Trimeric unit
x 6
x 4
Surfactant Protein A (SP-A)
Surfactant Protein D (SP-D)
Ribbon diagram of the structure of the recombinant fragment of SP-D.

Figure S2

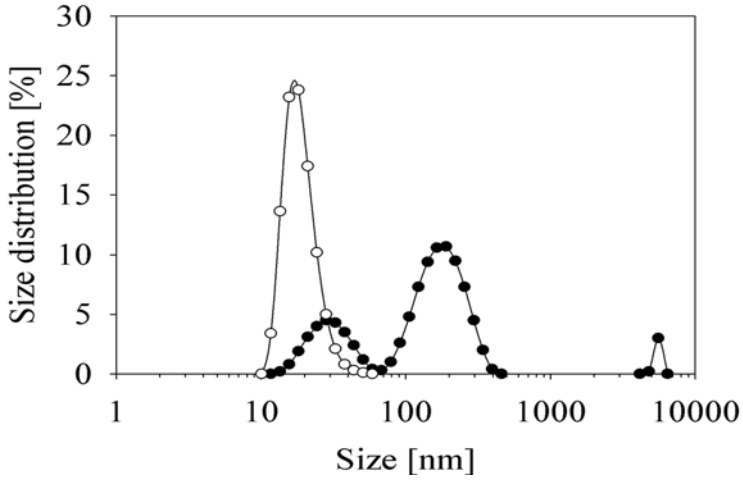

Figure S3

A) Size distributions of 100 nm U-PS + SP-A in water

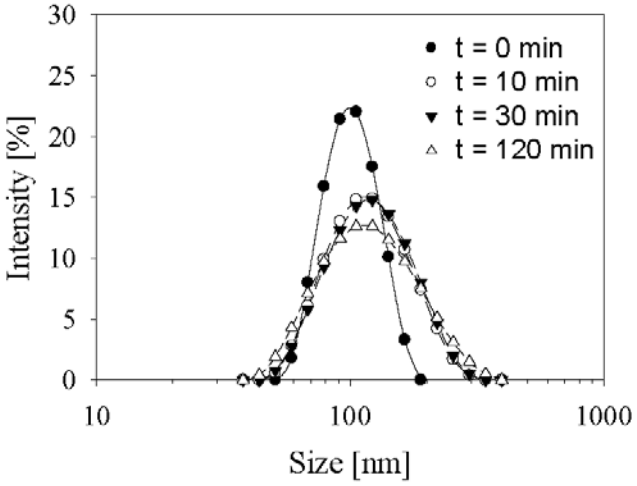

B) The effect of the calcium concentration on the size of 100 nm U-PS particles + SP-A over time

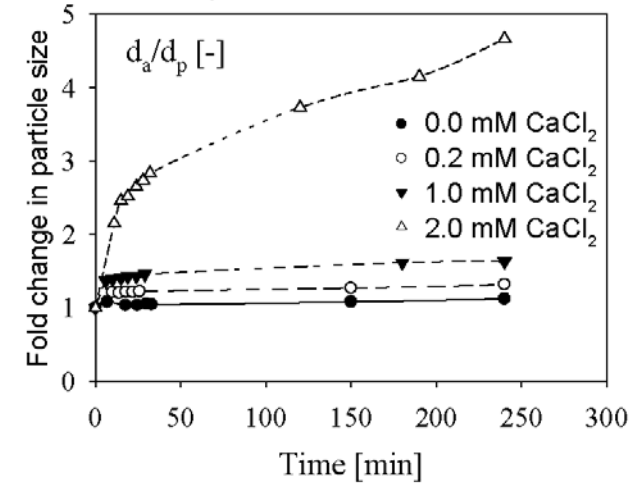

C) Size distributions of 100 nm U-PS + SP-A in water with calcium

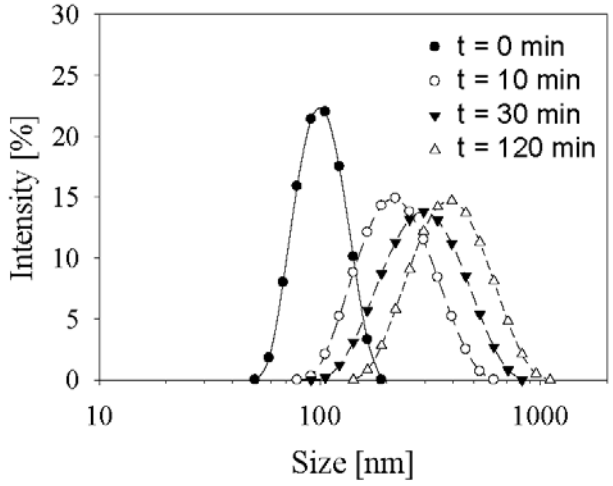

Figure S4

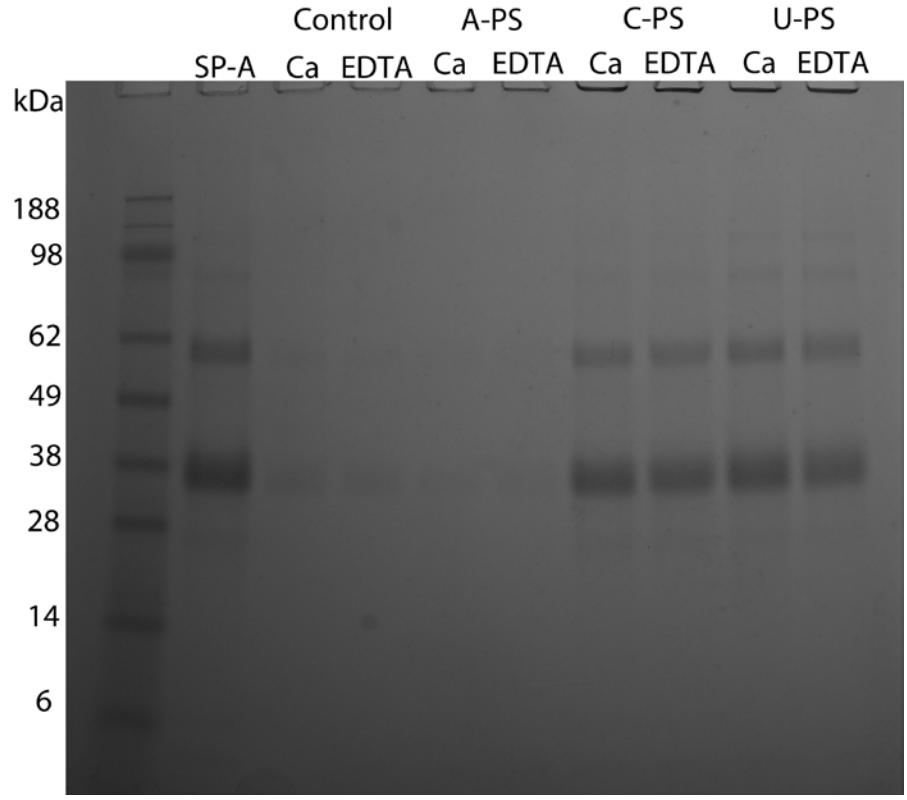
Control
A-PS
C-PS
U-PS
SP-A
Ca
EDTA
Ca
EDTA
Ca
EDTA
Ca
EDTA
kDa
188
98
62
49
38
28
14
6

Figure S5

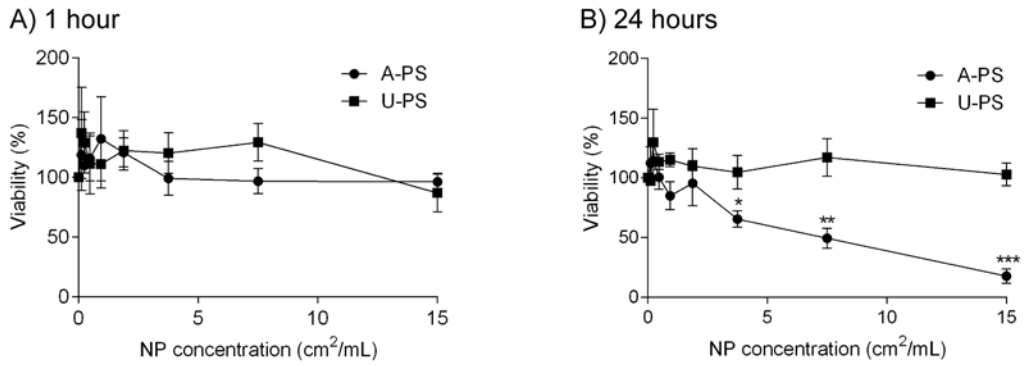

Figure S6

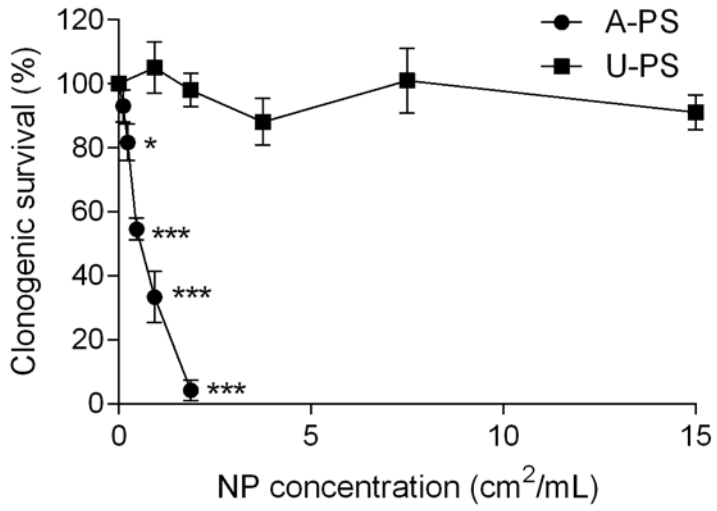
A-PS
U-PS
Clonogenic survival (%)
120
100
80
60
40
20
0
*
***
***
***
0
5
10
15
NP concentration (cm2/mL)

Table S1

NP	Zeta potential (mV)		Size (nm)		
	NP	NP + SP-A	t(min)	d2(nm)	Δd (%)
A-PS	+60	-22.8	0	100.6	-
			1400	150.0	49.1
U-PS	-38.5	-18.7	0	96.9	-
			20	100.4	3.6
			1440	110.7	14.3

Table S1: Size (intensity) and zeta potential of particles (2.5 cm^2/mL) before and after mixing with 10 µg/mL SP-A in water, Δd = (d(t)/d(t=0)). The zeta potential of 10 µg/mL SP-A alone was -11.8mV.